



**Fabrication and characterization of pristine and Pd
functionalized reduced graphene oxide for ammonia sensing**

Dr. NITIKA CHOUDHARY, DEPARTMENT OF PHYSICS

SHRI JAGDISHPRASAD JHABARMAL TIBREWALA UNIVERSITY

VIDYANAGARI, JHUNJHUNU, RAJASTHAN

SANGITA JAIN, Research scholar, physics, JJTU, JHUNJHUNU, RAJASTHAN

Abstract

A chemical sensor's sensing capability, stability, and specificity for detecting gases in a range of environments are important to the sensor's commercialization. We created highly selective ammonia sensors using Pd nanoparticles and reduced graphene oxide (rGO) nanocomposites. It was revealed that hierarchical nanoarchitectures may be created with excellent efficiency using a surfactant-free hydrothermal approach for the fabrication of sensing components. The generated rGO and Pd/rGO nanocomposite's structure, morphology, and electronic properties were examined using AFM, FESEM, and EDS technique. To further understand the detecting abilities of the sensors; dosage, temperature, and time-dependent ammonia and carbon monoxide sensing experiments were conducted on pure rGO and Pd/rGO nanocomposite sensors. The 2 wt. % Pd/rGO nanocomposite sensor achieved a sensor response of 97 percent at 100 °C, which is a seven fold increase over a pure rGO-based device. It was required to test the sensor's selectivity by exposing it to various reducing gases, such as carbon monoxide. When comparison to carbon monoxide, the sensor exhibited the strongest reactivity to ammonia. The current sensors' detecting capability implies that they might be employed for very selective ammonia detection, which is an exciting prospect.

1. Introduction

Graphene, a single layer of pure graphite composed of sp^2 hybridised carbon covalently bound to additional three atoms, has lately drawn the interest of researchers because of its unmatched physical, structural, chemical, and electronic capabilities [1-5]. The material's exceptional mechanical capacity, ultrafast energy transfer capability, and high surface area enable the substance to be used in future gas and vapor detectors with ultrafast response times and long-term longevity. Because pristine graphene is a 2-D substance, each carbon atom may be regarded as the surface atom, and hence each carbon atom site can be engaged in gas dynamics. This property of pristine graphene may ultimately account for its extremely sensitive sensor performance, with sensing techniques as low as a single molecule [6-8]. Additionally, the material's ease of functionalization, whether chemically or mechanically, enables bandgap engineering, which may result in a reasonable option to the specificity issues that plague chemical sensors. The newest advancements and fresh prospects in carbon materials gas and vapor detectors have been extensively examined in this study [9-14].

Single and few layered pristine graphene have been demonstrated to have a plethora of technical and scientific breakthroughs through unique nanodevice usage, the most significant of which being chemical and biosensors [15-18]. Electrons can travel at a million metres per second (mobility in the order of $210,000 \text{ cm}^2/\text{Vs}$) inside pristine graphene due to the easy sailing of electrons through the flawless honeycomb structure of pristine graphene. Each pristine graphene atom may be seen of as a surfaces atom designed to interact with the particle of the gas/vapor molecules, resulting in high sensor response. The ionic conductivity of pristine graphene varies significantly upon exposure to and subsequently adsorption of the targeted substances due to a change in the free electron. The amount of contact between the target gas/vapor particle may approach that of a single molecule, at which point the lowest quantum of consequent change in conductance may be detected in pristine graphene [16]. All these remarkable electronic features, combined with pristine graphene's enormous mechanical robustness, have elevated pristine graphene to a potential competitor as a future material for a variety of applications, including gas and VOC sensors [19-22].

Despite its great popularity as a result of recent significant improvements, the primary disadvantage of exfoliation is its 'poor productivity,' which precludes large-scale pristine graphene production necessary for batch manufacturing of devices. Another impediment is that the procedure is incompatible with current Si technology [23]. Nevertheless, the poor output may be compensated for by chemical treatment and CVD, and the incompatibility

issue with Si processing technologies resolved by epitaxy. As a result, such physical exfoliating techniques are useful when high-quality pristine graphene architecture preservation is needed. A big breakthrough was achieved lately in the field of chemical exfoliating when it was demonstrated that pure graphite might be gently exfoliate in the liquid state to provide defect-free single layer pristine graphene [25]. Although the technique has the potential to be scaled up to an industrial scale, it must first be resolved in order to address challenges such as thicknesses regulation of the pristine graphene sheets and repeatable manufacture of large-area pristine graphene. A novel technique for dispersing pure graphite in micellar solutions has been developed, which makes use of ultrasonography to do this [26-30]. Because of this, wide-scale exfoliation occurs, resulting in huge volumes of multi-layered pristine graphene with much less than five layers and small amounts of single layer pristine graphene being produced. As a result of the adsorbed surfactants molecule ions, the exfoliated grains are stabilised against reaggregation by the action of Coulomb interaction. After proving to be effective, this technology has garnered the attention of the semiconductor industry as a feasible approach for the post-CMOS era.

When it comes to gas/VOC sensors, the ultimate goal ought to be the identification of a specific species with the ability to sense to the level of an individual element or compound. GO has an exceptionally large surface/volume ratio, allowing it to detect small amounts of target gases [31-34]. The range of sensitivity for pristine graphene detectors can vary anywhere from one individual atom to extremely high dosage levels. Furthermore, due to its mechanical resilience, pristine graphene, in contrast to carbon nanotubes, does not endanger its 2-D delocalized conduction capabilities due to its mechanical robustness. The sensor signal's electronic and mechanical qualities may be easily utilized in order to execute the transduction of the information.

Because fundamental pristine graphene does not have any dangling bonds which is highly desired for gas/vapor reaction and hence does not increase the adsorption of compounds on pristine graphene sheets, as previously stated, natural pristine graphene poses a challenge [35-37]. As a result, pristine graphene must be designed and synthesized with polymers. The thin functional coating of improves the adhesion of target gases, resulting in a substantial change in the baseline resistance. In the field of chemical sensor study, doping/surface alteration, particularly by noble metallic ions, has long been long recognised. When using pristine graphene, the specific benefit is that it has extraordinarily high conductivity and noise cancelling, which allows for the detection of changes in baseline resistance even at levels as low as ppm and ppb of the specific species [38-42]. In addition,

functionalization of reduced GO can be used to improve chemical affinity and specificity in a variety of applications. In the presence of the carrier, there is a local shift in carrier concentration [43].

To increase the sensing capability of graphene, several distinct forms of oxidised pristine graphene have been researched in the past. When the device is tested both in reducing and oxidising situations, it exhibits a normal p-type response as expected. In addition, by altering the temperature range and oxygen levels, the particular reaction to NO₂ was investigated. GO was shown to have significant sensing activity, which was demonstrated to be mostly due to surface oxygen units. As a result, this demonstrates the adaptability of pristine GO in gas/VOC detection [44-48]. It has been discovered that the substrate for fabricating pristine graphene-based chemical sensors is an important and challenging parameters of the sensors [49].

The study of fabricating pristine graphene is developing at a breakneck pace around the world, and notable academics have reported on the material's excellent tensile, electrical, photonic, and magnetic capabilities. It is unquestionably an indication of the favourable futuristic characteristics of the usage of pristine graphene on a wide scale [50-52]. Processability, doping capability, compact device designs, and compatibility with a range of surfaces can render pristine graphene a nearly ideal material. In order to assess the potential use of pure graphene for realistic chemical gas detection and large applications in the future, further efforts will be required in the future to transfer laboratory research results to field operations.

2. Experimental work

To complete the synthesis, graphite powder (99 percent purity), palladium chloride (99 percent purity), sodium hydroxide (99 percent purity), potassium permanganate, hydrogen peroxide, ethanol and methanol, sulphuric acid, and hydrochloric acid were all used as solvents. All of the chemicals were acquired from Alfa Aesar and were utilized without any additional purification or processing.

Graphene oxide (GO) was manufactured from natural graphite using a modified Hummer's process, according to the researchers. The following steps were followed: 5 g of graphite was combined with 0.5 g of sodium hydroxide, then 20 ml of sulphuric acid was added while the mixture was being stirred continuously. In order to avoid overheating, 8 g of potassium permanganate was progressively added to the aforesaid solution over a period of 2 hours while maintaining the temperature below 50 °C to avoid overheating. At 50 °C, the

mixture was vigorously swirled for 10 hours, and the resultant solution was diluted by adding 200 millilitres of water while vigorously swirling. Further treatment with a 20 percent hydrogen peroxide solution was performed after the potassium permanganate reaction was completed to guarantee that the reaction was completed. The GO nanosheets were produced by rinsing the mixture in HCl and deionized water, followed by filtering and drying, and then drying again. The following is a description of the hydrothermal technique used to create rGO-Pd nanocomposites. First, the needed quantity of the produced graphene oxide was sonicated and immersed into deionized water. Afterwards, 0.02 g of palladium chloride was mixed in the resulting dispersion by continuous stirring for 30 minutes to yield 1 weight percent, 2 weight percent, and 3 weight percent of rGO loaded Pd, 0.05 g of sodium hydroxide was added to this solution while it was being stirred continuously. Afterward, the mixed suspension has been sealed in a 200-mL Teflon container with an enclosure made of steel and sent to the furnace for another 30-minutes period. The reaction was conducted at 200 °C for 2 hours. Once the precipitate had been allowed to reach normal temperature, it was recovered using sonification and then washed multiple times with water and ethanol. The solid products that were obtained were dried at 200 °C in preparation for further examination.

Fabrication of sensor devices by the screen printing process: In a typical fabrication, the pristine rGO and Pd/rGO sensitive layer was formed by diluting the synthesised nanocomposite with 40 weight percent of copolymers that consisted of PMMA-PMBA as binder and BCA as solvent for 3 hours, followed by drying the pristine rGO and Pd/rGO sensitive layer. The following dimensions were used to create the screen for the interdigitated electrode (IDE) and silver paste was screen-printed onto a prepared Si substrate and dried at 200 °C for 10 minutes after being applied to the substrate. The test gases used were ammonia (5-120 ppm) and carbon monoxide (20-200 ppm).

3. Results and Discussion

i. Material characterization results

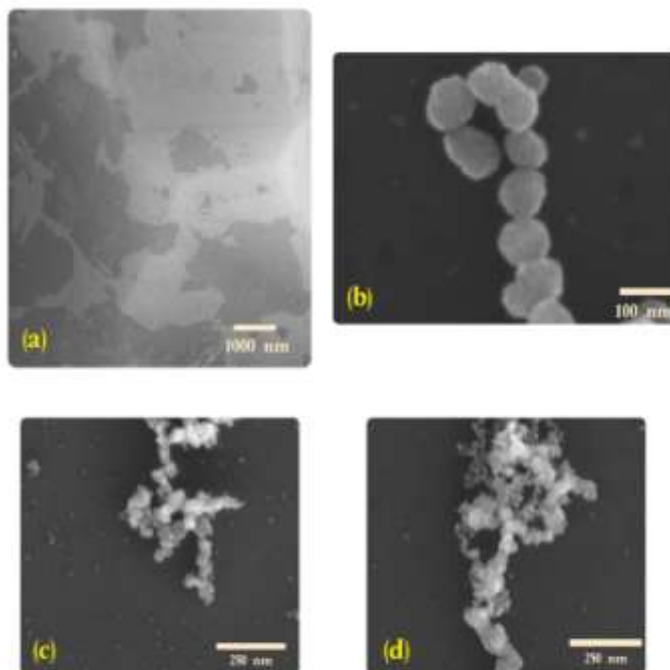


Fig. 1 SEM images of : (a) Pristine reduced graphene oxide (rGO), (b) 1 wt% Pd functionalized rGO, (c) 2 wt% Pd functionalized rGO, and (d) 3 wt% Pd functionalized rGO

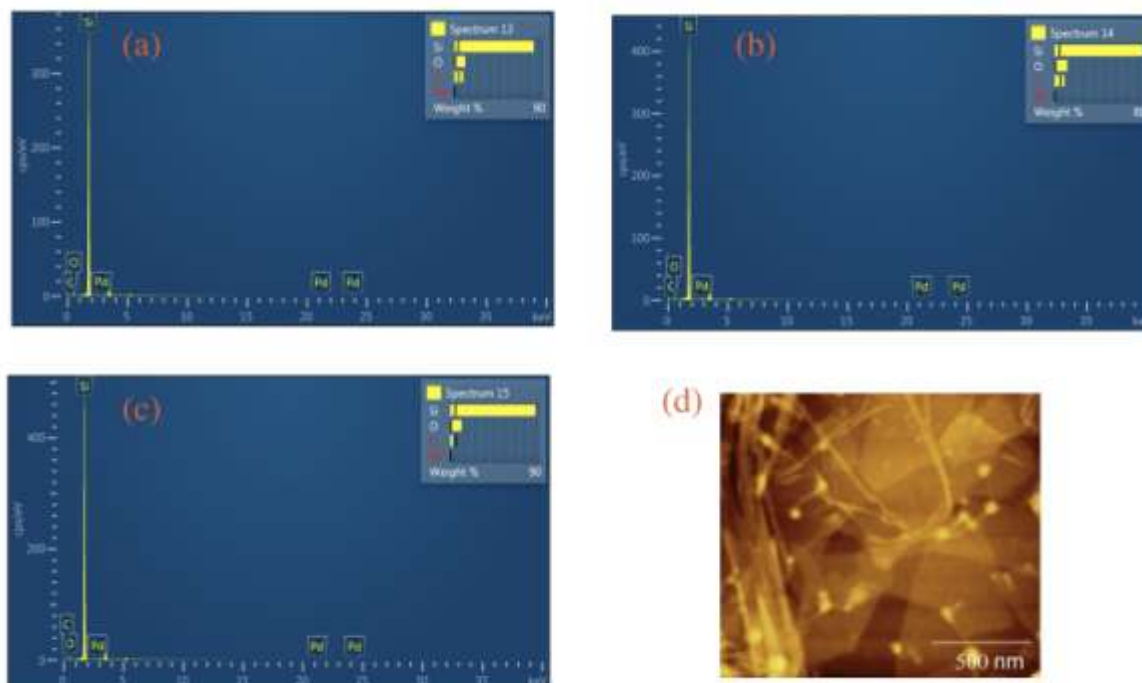


Fig. 2EDS spectrum of : (a) 1 wt% Pd functionalized rGO, (b) 2 wt% Pd functionalized rGO, and (c) 3 wt% Pd functionalized rGO; (d) AFM of 3 wt. % Pd functionalized rGO

The FESEM picture of GO shows that the average thickness of the graphene sheets is 34 nm, and the no Pd nanoparticles were visible in the image (Fig. 1 (a)). The FESEM images of (Fig. 1 (b-d)) the material may be used to determine the influence of Pd nanoparticle dosage on the development of Pd-rGO nanocomposites in the first step of the investigation. It is possible to visualise the Pd-rGO nanocomposites with just little overlap of the rGO sheets when using the 1 wt. percent rGO sample with only a few merging of the rGO sheets. The average diameter of Pd nanoparticles were computed to be 65 nm. It was discovered that when the dosage of Pd was raised to 2 wt. covered the whole surface of the rGO sheets and average diameter of nanoparticles were in the order of 60-65 nm.

The EDS spectrum of as grown rGO and Pd functionalized rGO samples obtained is illustrated in Fig. 2 (a-c). The spectrum reveals the presence of silicon, carbon, oxygen, and palladium elements only. Thus, spectrum gives clear evidence for presence of Pd in the doped samples. Fig. 2 (a) shows the EDS spectrum of 1 wt. % Pd doped rGO. The C/O ratio obtained in Fig. 2 (a) was 55/45 with Pd dosage of 0.98 %. Fig.2 (b) shows the EDS spectrum of 2 wt. % Pd doped rGO. The C/O ratio obtained in Fig. 2 (b) was 54/46 with Pd dosage of 1.98%. Fig. 2 (c) shows the EDS spectrum of 3 wt. % Pd doped rGO. The C/O ratio obtained in Fig. 2 (c) was 50/50 with Pd dosage of 3 %. Fig. 2 (d) also shows AFM result of 3 wt. % Pd functionalized rGO. Thus, above characterization results demonstrated a clear growth of Pd nanoparticles over rGO sheets and these samples were used to study gas sensing of ammonia and carbon monoxide in the next step.

ii. Determining optimal functioning temperature of GO sensors

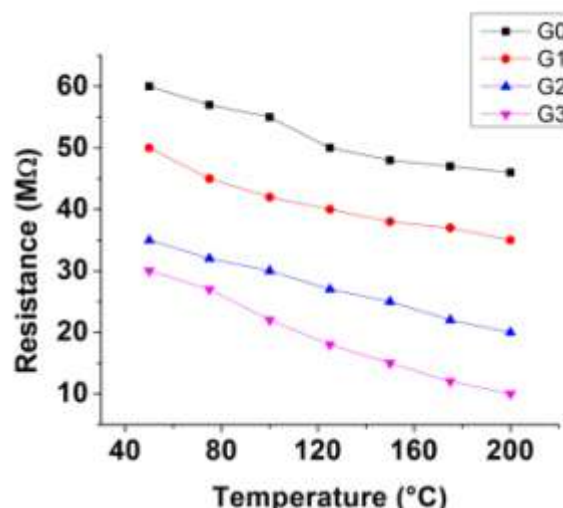


Fig. 3 Baseline resistance of four sensors (G0-G4) vs operating temperate plot in air ambient

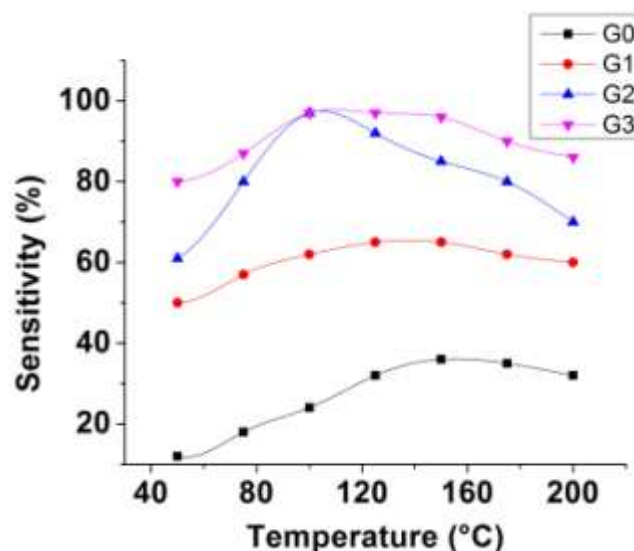


Fig. 4 Sensitivity of four sensors (G0-G4) vs operating temperature plot in 200 ppm ammonia ambient

The baseline resistance of reduced GO (rGO) based sensor in air ambient was evaluated for a span of operational temperature (50 °C - 200 °C) as illustrated in Fig. 3. It was established out that the baseline resistance of reduced GO based sensor was decreased from 60 MΩ to 46 MΩ as functioning temperature has been stepped up from 50 °C to 200 °C. It is evident that density of charge carriers increases as functioning temperature elevates in the reduced GO. This results in the decrease in the baseline resistance of material as observed from the Fig. 3. Following this, the sensitivity of rGO sensor was evaluated for a span of operational temperature (50 °C - 200 °C) as illustrated in Fig. 4. The sensitivity was noted to be stepped up from 12% to 36 % as functioning temperature was surged from 50 °C to 150 °C and then hovered in between 32-35% when temp was set in between 150-200 °C. Thus, the ideal functioning temperature for rGO sensor was computed to be 150 °C. The response and recovery/retrieval time of reduced GO sensor towards 200 ppm dosage of ammonia gas over a extent of functioning temperature of 50 °C to 200 °C was also investigated. Choosing the prime operational temperature for gas sensors is a crucial step which determines the overall sensing performance of the sensor. Taking into account the sensitivity, response span and recovery span of sensor device at various operational temperatures, 150 °C was selected as the prime operational temperature for the rGO sensor. At this functioning temperature, a maximum sensitivity of 36% was evaluated with a 25 and 19 sec of response and recovery

duration respectively. As a result, further investigations at this temperature of 150 °C were conducted for measuring sensitivity, response duration and recovery duration using various doses of ammonia and carbon monoxide.

The baseline resistance of 1 wt. % Pd functionalized rGO sensor was evaluated for a span of functioning temperature (50 °C- 200 °C) illustrated in Fig. 3. It was established out that the baseline resistance of sensor device was decreased from 50 MΩ to 35 MΩ as functioning temperature was stepped up from 50 °C to 200 °C. It is evident that number of charge carriers increases as functioning temperature increases in semiconductor. However, for 1 wt. % Pd functionalized rGO, the baseline resistance was found to be lower than that of rGO because of doping. As Pd is metallic in nature with high electron dosage and by adding 1 wt. % of Pd into rGO, the overall electron dosage of material gets elevated. Therefore, the baseline resistance of device after introduction of Pd nanoparticles when evaluated at 50 °C gets reduced from 60 MΩ to 50 MΩ. Also, further increment in functioning temperature reduces the baseline resistance of 1 wt. % Pd functionalized rGO but with smaller rate as evident from the slope of baseline resistance vs functioning temperature graph. The slope of 1 wt. % Pd functionalized rGO has less steeper slope than that of pristine rGO suggesting less dependence of Pd functionalized rGO's baseline resistance towards functioning temperature. The sensitivity of 1 wt. % Pd functionalized rGO sensor was evaluated for a span of functioning temperature from 50 °C to 200 °C as illustrated in Fig. 4. The sensitivity was noted to be stepped up from 50 % to 65 % as functioning temperature was stepped up from 50 °C to 125 °C, gets saturated at 65 % from 125 °C to 150 °C, but gets decreased from 65 % to 60 % when operated between 150 °C to 200 °C. Thus, prime functioning temperature for rGO sensor was computed to be 125 °C. Taking into account the sensitivity, response duration, and recovery duration at various functioning temperatures, 125 °C was selected as the prime temperature for the 1 wt. % Pd functionalized rGO sensor. At this functioning temperature, a maximum sensitivity of 65 % was obtained with a shorter response and recovery duration (24 and 20 sec).

The baseline resistance of 2 wt. % Pd functionalized rGO sensor was evaluated for an order of functioning temperature (50 °C to 200 °C) as illustrated in Fig. 3. It was established out that baseline resistance of rGO sensor functionalized with 2 wt. % of Pd sensor was reduced from 35 MΩ to 20 MΩ as functioning temperature was stepped up from 50 °C to 200 °C. The sensitivity of 2 wt. % Pd functionalized rGO sensor was evaluated for a span of functioning temperature from 50 °C to 200 °C illustrated in Fig. 4. The sensitivity was noted to be stepped up from 61 % to 97 % as functioning temperature was stepped up from 50 °C to

100 °C and gets reduced when operated in between 100 °C to 200 °C. Thus, the operational temperature of sensor device was computed to be 100 °C. At this functioning temperature, a maximum sensitivity of 97 % was obtained with a shorter response and recovery duration (12 and 30 sec).

The baseline resistance of 3 wt. % Pd functionalized rGO sensor was evaluated for a span of functioning temperature from 50 °C to 200 °C as illustrated in Fig. 3. It was established out that the baseline resistance of sensor device was decreased from 30 MΩ to 10 MΩ as functioning temperature was stepped up from 50 °C to 200 °C. The sensitivity of 3 wt. % Pd functionalized rGO sensor was evaluated for a span of functioning temperature from 50 °C to 200 °C as illustrated in Fig. 4. The sensitivity was noted to be stepped up from 80 % to 97 % as functioning temperature was stepped up from 50 °C to 100 °C and gets reduced from 97 % to 86 % when operated in between 100 °C to 200 °C. Thus, the optimum functioning temperature for rGO sensor was computed to be 100 °C. At this functioning temperature, a maximum sensitivity of 97 % was obtained with a shorter response and recovery duration (16 and 13 sec).

iii. Gas sensing results

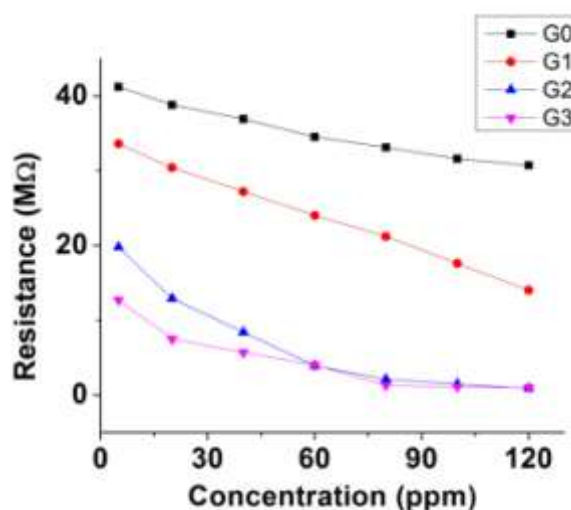


Fig. 5 Baseline resistance of four sensors (G0-G4) vs ammonia concentration (5-120 ppm)

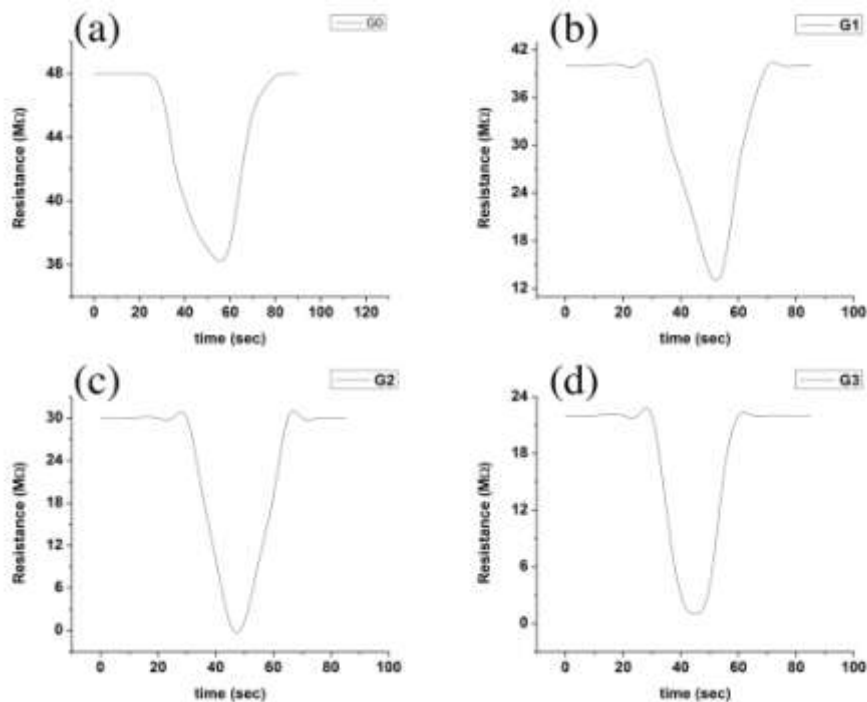


Fig. 6 Transient response of four sensors (G0-G4) upon exposure to 200 ppm of ammonia

Fig. 5 shows the change in the baseline resistance of all four sensors when operated at different ammonia dosage ranging from 5-120 ppm. The transient response of rGO sensor (G0) towards 200 ppm dosage of ammonia was investigated at its prime operational temperature (150 °C) as illustrated in Fig. 6. The baseline resistance of sensor device was decreased from 48 MΩ to 35 MΩ. The response and recovery duration were computed to be 25 sec and 19 sec respectively. Fig. 6 illustrates the sensor's transient response in the vicinity of 120 ppm of ammonia dosage when operated at its optimum functioning temperature of 125 °C. The baseline resistance of 1 wt. % Pd functionalized rGO (G1) sensor device was decreased from 40 MΩ to 14 MΩ. Also, the response and recovery duration were computed to be 24 sec and 20 sec respectively. The transient response of 2 wt. % Pd functionalized rGO (G2) sensor towards 120 ppm dosage of ammonia was investigated at its prime operational temperature (100 °C) as illustrated in Fig. 6. The baseline resistance of the sensor device was decreased from 35 MΩ to 0.9 MΩ. The response and recovery duration were also computed to be 12 sec and 22 sec respectively. The transient response of the 3 wt. % Pd functionalized rGO (G3) sensor upon exposure to ammonia gas dosage of 120 ppm was evaluated as illustrated in Fig. 6. The baseline resistance of the sensor was decreased from 30 MΩ to 3 MΩ upon exposure to 120 ppm dosage of ammonia. The corresponding response and recovery duration was evaluated as 16 sec and 13 sec respectively.

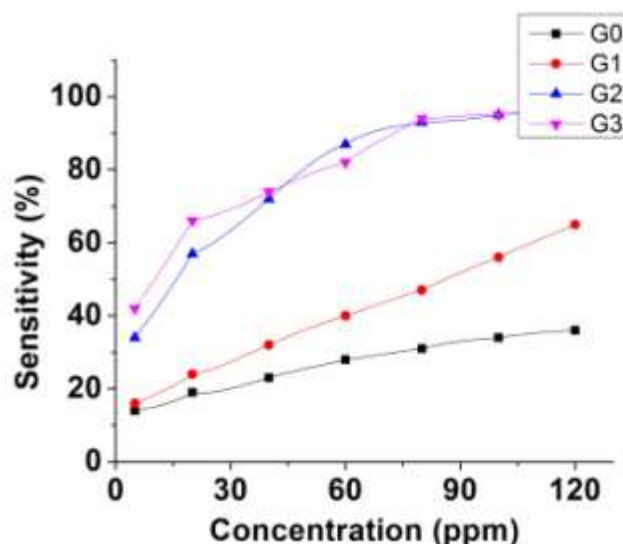


Fig.7 Sensitivity of four sensors (G0-G4) vs ammonia concentration (5-120 ppm)

Fig. 7 illustrates the rGO (G0) sensor's response towards various dosages (25-200 ppm) of ammonia gas. The dosage dependent experiments revealed that the sensor had a maximum sensitivity of 36 % towards 200 ppm dosage of ammonia. The lower detection limit of the sensor is defined as the dosage level where sensitivity of the sensor becomes more than 10 %. It was established out that rGO sensor was capable of detecting ammonia concentrations of as low as 20 ppm. For 1 wt. % Pd functionalized rGO (G1) sensor, the dosage-dependent experiments conducted at the prime functioning temperature of 125 °C as illustrated in Fig. 7 revealed the lowest gas detection limit of 1 ppm with a sensitivity of 10 %. The sensor recorded the highest response at dosage of 120 ppm with a sensitivity of 65 %. For 1 wt. % Pd functionalized rGO (G2) sensor, the dosage dependent experiments revealed that the sensor had a maximum sensitivity of 97 % towards 120 ppm dosage of ammonia. It was established out that 2 wt. % Pd functionalized rGO sensor was capable of detecting ammonia concentrations of as low as 500 ppb. Fig. 7 also illustrates the dosage dependent investigations of 3 wt. % Pd functionalized rGO (G3) sensor at the prime functioning temperature of 100 °C. The sensor was reported to have a lowest detectable dosage of 400 ppb and a maximum detectable dosage of 120 ppm with a response of 97 %.

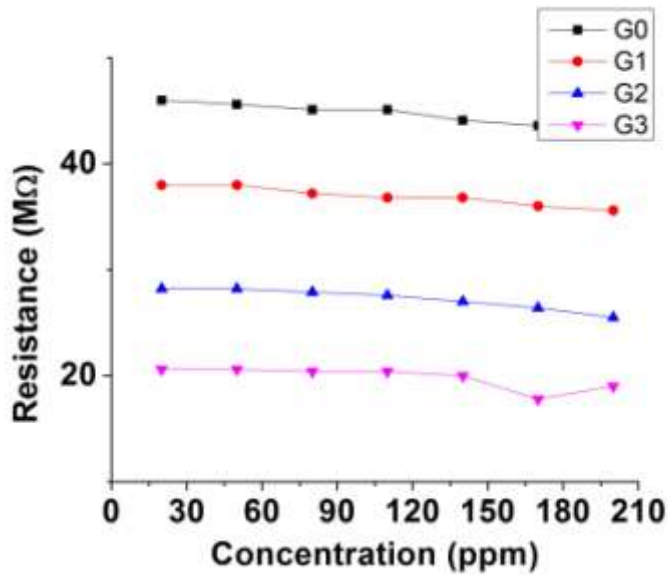


Fig. 8 Baseline resistance of four sensors (G0-G4) vs carbon monoxide concentration (20-200 ppm)

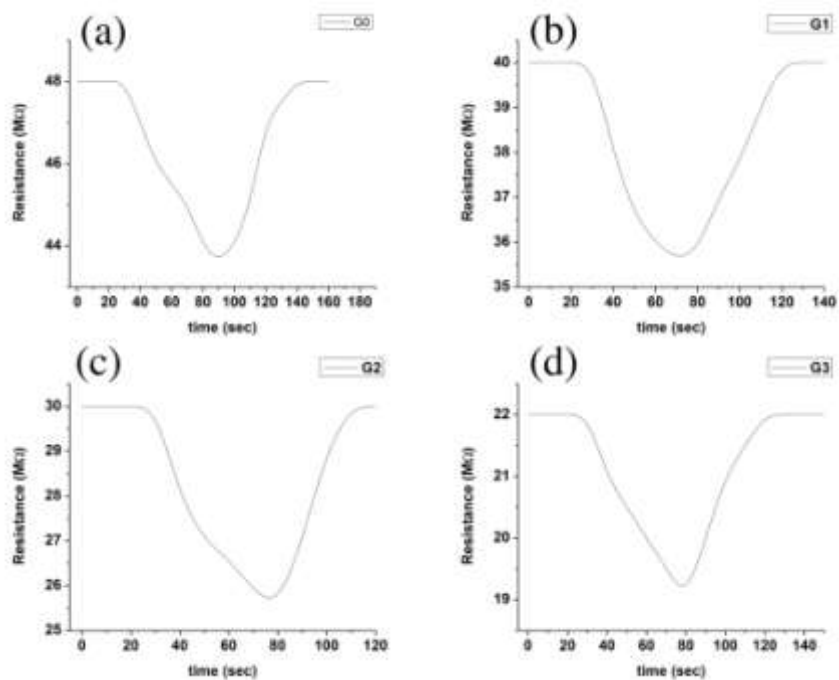


Fig. 9 Transient response of four sensors (G0-G4) upon exposure to 200 ppm of carbon monoxide

Fig. 8 shows the change in the baseline resistance of all four sensors when operated at different carbon monoxide dosage ranging from 20-200 ppm. The transient response of rGO

sensor towards 200 ppm dosage of carbon monoxide was investigated at its prime operational temperature (150 °C) as illustrated in Fig. 9. The baseline resistance of device was decreased from 50 MΩ to 43.6 MΩ. The response and recovery duration were computed to be 58 sec and 48 sec respectively. Fig. 9 illustrates the sensor's transient response in the vicinity of 200 ppm dosage of carbon monoxide dosage when operated at its optimum functioning temperature of 125 °C. The baseline resistance of sensor device was decreased from 50 MΩ to 36 MΩ. Also, the reaction and restoration duration were computed to be 45 sec and 25 sec respectively. The transient response of the 2 wt. % Pd functionalized rGO sensor upon exposure to carbon monoxide gas dosage of 200 ppm was evaluated as illustrated in Fig. 9. The baseline resistance of the device was decreased from 30 MΩ to 25 MΩ upon exposure to 200 ppm dosage of carbon monoxide. The corresponding response and recovery duration was evaluated as 52 sec and 25 sec respectively. The transient response of the 3 wt. % Pd functionalized rGO sensor upon exposure to carbon monoxide gas dosage of 200 ppm was evaluated as illustrated in Fig. 9. The baseline resistance of the sensor device was decreased from 30 MΩ to 19 MΩ upon exposure to 200 ppm dosage of carbon monoxide. The corresponding response and recovery duration was evaluated as 55 sec and 22 sec respectively.

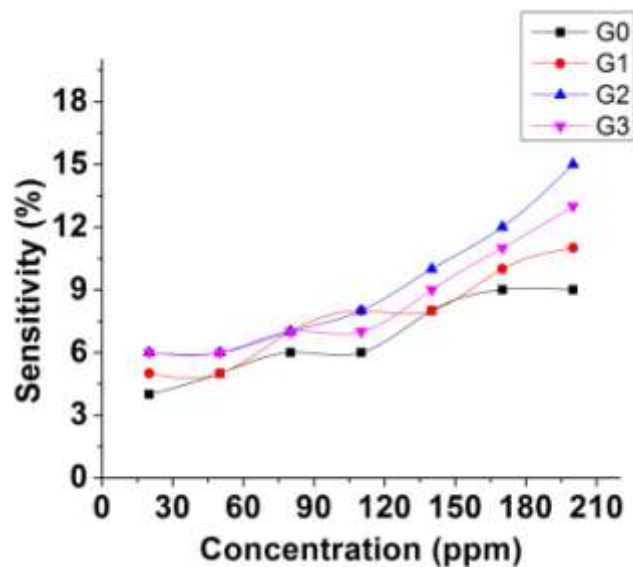


Fig. 10 Sensitivity of four sensors (G0-G4) vs carbon monoxide concentration (20-200 ppm)

Fig. 10 illustrates the rGO (G0) sensor's response towards various concentrations (25-200 ppm) of carbon monoxide. The dosage dependent experiments revealed that the sensor

device had a maximum sensitivity of 9 % towards 200 ppm dosage of carbon monoxide. It was established out that rGO (G0) sensor device was not capable of efficiently detecting carbon monoxide dosages below 220 ppm. Fig. 10 illustrates the 1 wt. % Pd functionalized rGO(G1) sensor's response towards various concentrations (25-200 ppm) of carbon monoxide. The dosage-dependent experiments conducted at the prime functioning temperature of 125 °C revealed the lowest gas detection concentration limit of 170 ppm at a sensitivity of 10 %. The sensor recorded the highest sensitivity at 200 ppm with a sensitivity of 11 %. Fig. 10 illustrates the dosage dependent investigations of 2 wt. % Pd functionalized rGO(G2) sensor device at the prime functioning temperature of 100 °C. The sensor was reported to have a lowest detectable dosage of 140 ppm. The sensitivity of the sensor increased from 6 % to 15 % upon exposure to 25-200 ppm dosage of carbon monoxide. Fig. 10 illustrates the dosage dependent investigations of 3 wt. % Pd functionalized rGO(G3) sensor device at the prime functioning temperature of 100 °C. The sensor was reported to have a lowest detectable dosage of 150 ppm. The sensitivity of the sensor increased from 6 % to 13 % upon exposure to 20-200 ppm dosage of carbon monoxide.

iv. Sensing mechanism

The sensing method uses surface conduction that is changed by molecules that have been adsorbed on rGO [53]. This changes the space-charge layer as well as the surface states induced by molecules. One way that a gas species can get on top of a sensor material is by adhering to it. Another way is by exchanging electrons: chemisorption. This is the transfer of electrons that happens when the gas species is attached to a surface. The primary distinction processes is that physical adsorption process is a process that releases heat, while chemical adsorption is a process that releases heat. The chemisorbed oxygen, water, and/or the hydroxyl ions that are found on surfaces can help with the charge transfer between gas species, but this isn't always the case. Because of its higher ionization energy and low density, oxygen is the least energetic of the three that we looked at in this study.

When a reducing agent, is added, the O_2 evaporates faster than the O^- , which means that O^- has more power in the reaction than the O_2 . A reducing agent may respond with the lattice air, O_2 , when it comes into the room. Adsorbed oxygen is thought to transport an electron from rGO to chemisorbed oxygen. Since rGO has more hydroxyl groups, the number of electrons in the conductance band has risen. This has led to the depletion layer growing in this study. Oxygen is attached to OH^- , which induces an oxygen ion to be established on the material surface. This oxygen ion stays on the material surface and changes into other aspects

of anionic oxygen by taking charged particles from the conduction band. Nature's non-reversible processes, like the producing of atomic/ionic oxygen in situ, are inferred by the methodologies that are shown in this text. charged oxidants that have bonded to grain boundaries are to blame for some of the things that happen when there is space charge and band modulation. It is thought that changes in the chemisorbed molecule dosage are the main source of the electrical reaction, while the rGO phase stays highly stable as a result. Theory shows that gas molecules don't stick very well to perfect graphene surfaces, but they stick better to imperfect graphene surfaces [55-58]. The conductivity of graphene-based equipment, such as gas sensors, can be affected by flaws and other types of groups. If the HOMO and LUMO positions of the adsorptive ammonia molecules are close to each other, the orientation of charge transfer can be changed in graphene. In other words, the charge-transfer sites are not determined by the charge-transfer sites taken by individual, but by how the particles are oriented with regard to the surface of the cell. There are differences in the orbital overlap between both the HOMO of the ammonia particle and the HOMO of graphene. It doesn't seem like the LUMO, which is nearer to the Dirac point than the HOMO, has any effect on the electron doping process, even though it is closer to the point.

The process of breaking down analytes into CO₂ and water in the presence of various adsorbates has many steps [54-58]. Adjustments in charge distribution or motion, or both, needs to be the source of the transformation in conductance because conductance is connected to the combination of charge density and mobility. The adsorption of gas is caused by the graphene's linear band structure at the Dirac points. This could lead to more electrons because the gas is a source of electrons. Ammonia and other closed-shell adsorbates don't change the band structure of graphene like other closed-shell adsorbates do. Instead, they affect the distribution of charges within graphene. There are many "surface impurities," but when they were between graphene and the surface, they can cause indirect graphene doping.

4. Conclusion

The Pd/rGO nanocomposites were synthesized utilising a straightforward hydrothermal technique that did not need the use of surfactants. The morphological and structural studies conducted on the rGO sheets demonstrate that the technique utilized to fabricate the sheets is effective in producing crystalline Pd nanoparticles that are suitable for usage in the graphene sheets. When the nanocomposites were operated at 100 °C, the 2 wt. % Pd functionalized rGO sensor exhibited a sensor response from 34% to 97% . upon exposure to 5-120 ppm of ammonia. However, for carbon monoxide sensing, the same sensor exhibited a

sensor response of 15 % for 200 ppm of carbon monoxide. Thus, Ti functionalized rGO sensor demonstrated ammonia gas selective nature. The response and recovery characteristics, in addition, demonstrated a significant variation from the prior findings. Pd/rGO is a nanocomposite sensor that can detect ammonia in 12 seconds and recover to 120 ppm in 22 seconds at 100 °C. As a result, utilising well-designed Pd/rGO nanocomposite sensors for practical ammonia sensors is a viable approach that has the potential to provide positive results.

References

1. K.S. Novoselov, A.K. Geim, S.V. Morozov, D. Jiang, Y. Zhang, S.V. Dubonos, I.V. Grigorieva, A.A. Firsov, Electric field effect in atomically thin carbon films, *Science* 306 (2004) 666–669.
2. E.W. Hill, A. Vijayaraghavan, K. Novoselov, Graphene sensors, *IEEE Sensors Journal* 11 (2011) 3161–3170.
3. L. Gomez De Arco, Y. Zhang, C.W. Schlenker, K. Ryu, M.E. Thompson, C. Zhou, Continuous, highly flexible, and transparent graphene films by chemical vapor deposition for organic photovoltaics, *ACS Nano* 4 (2010) 2865–2873
4. J. Wintterlin, M.L. Bocquet, Graphene on metal surfaces, *Surface Science* 603 (2009) 1841–1852.
5. A.K. Geim, K.S. Novoselov, The rise of graphene, *Nature Materials* 6 (2007) 183–191.
6. Y.Si, E.T.Samulski, Synthesis of water soluble graphene, *Nano Letters* 8 (2008) 1679–1682.
7. V. Singh, D. Joung, L. Zhai, S. Das, S.I. Khondaker, S. Seal, Graphene based materials: past, present and future, *Progress in Materials Science* 56 (2011) 1178–1271.
8. Y. Zhu, S. Murali, W. Cai, X. Li, J.W. Suk, J.R. Potts, R.S. Ruoff, Graphene and graphene oxide: synthesis, properties and applications, *Advanced Materials* 22 (2010) 3906–3924.
9. M. Dragoman, D. Dragoman, Graphene-based quantum electronics, *Progress in Quantum Electronics* 33 (2009) 165–214.
10. R.R. Nair, P. Blake, A.N. Grigorenko, K.S. Novoselov, T.J. Booth, T. Stauber, N.M.R. Peres, A.K. Geim, Fine structure constant defines visual transparency of graphene, *Science* 320 (2008) 1308–1312.
11. K.S. Kim, Y. Zhao, H. Jang, S.Y. Lee, J.M. Kim, K.S. Kim, J.H. Ahn, P. Kim, J. Choi, B.H. Hong, Large-scale pattern growth of graphene films for stretchable transparent

- electrodes, *Nature* 457 (2009) 706–711.
12. C. Lee, X. Wei, J.W. Kysar, J. Hone, Measurement of the elastic properties and intrinsic strength of monolayer graphene, *Science* 321 (2008) 385–388.
 13. S.K. Pati, T. Enoki, C.N.R. Rao (Eds.), *Graphene and Its Fascinating Attributes*, World Scientific Publishing Co Pvt. Ltd., Singapore, 2011.
 14. H. Raza (Ed.), *Graphene Nanoelectronics: Metrology, Synthesis, Properties and Applications*, Springer, Berlin, Germany, 2012.
 15. W. Choi, I. Lahiri, R. Seelaboyina, Y.S. Kang, Synthesis of graphene and its applications: a review, *Critical Reviews in Solid State and Materials Sciences* 35 (2010) 52–71.
 16. H. Shioyama, Cleavage of graphite to graphene, *Journal of Material Science Letters* 20 (2001) 499–500.
 17. M.J. Allen, V.C. Tung, L. Gomez De Arco, Z. Xu, L.M. Chen, K.S. Nelson, C. Zhou, R.B. Kaner, Y. Yang, Soft transfer printing of chemically converted graphene, *Advanced Materials* 21 (2009) 2098–2102.
 18. R.V. Gorbachev, A.S. Mayorov, A.K. Savchenko, D.W. Horsell, F. Guinea, Conductance of p-n-p graphene structures with air-bridge top gates, *Nano Letters* 8 (2008) 1995–1999.
 19. M.F. Craciun, S. Russo, M. Yamamoto, S. Tarucha, Tuneable electronic properties in graphene, *Nano Today* 6 (2011) 42–60.
 20. K.S. Novoselov, A.K. Geim, S.V. Morozov, D. Jiang, M.I. Katsnelson, I.V. Grigorieva, S.V. Dubonos, A.A. Firsov, Two-dimensional gas of mass less Dirac fermions in graphene, *Nature* 438 (2005) 197–200.
 21. M. Acik, Y.J. Chabal, Nature of graphene edges: a review, *Japanese Journal of Applied Physics* 50 (2011) 070101–0701016.
 22. V.V. Cheianov, V. Falko, B.L. Altshuler, The focusing of electron flow and a Veselago lens in graphene p-n junctions, *Science* 315 (2007) 1252–1255. [22] A.K. Geim, Graphene: status and prospects, *Science* 324 (2009) 1530–1534.
 23. N. Tombros, C. Jozsa, M. Popinciuc, H. Jonkman, B. van Wees, Electronic spin transport and spin precession in single graphene layers at room temperature, *Nature* 448 (2007) 571–575.
 24. T. Kuila, S. Bose, P. Khanra, A.K. Mishra, N.H. Kim, J.H. Lee, Recent advances in graphene-based biosensors, *Biosensors and Bioelectronics* 26 (2011) 4637–4648.
 25. W. Choi, J.W. Lee (Eds.), *Graphene: Synthesis and Applications*, CRC Press (Taylor

- and Francis group), New York, USA, 2012.
26. H.E. Chan (Ed.), *Graphene and Graphite Materials*, Nova Science Publishers Inc., New York, USA, 2010.
 27. M. Pumera, A. Ambrosi, A. Bonanni, E.L.K. Chng, H.L. Poh, Graphene for electrochemical sensing and biosensing, *Trends in Analytical Chemistry* 29 (2010) 954–965.
 28. E. Rokuta, Y. Hasegawa, A. Itoh, K. Yamashita, T. Tanaka, S. Otani, C. Oshima, Vibrational spectra of the monolayer films of hexagonal boron nitride and graphite on faceted Ni(755), *Surface Science* 427 (1999) 97–101.
 29. K.S. Novoselov, D. Jiang, F. Schedin, T.J. Booth, V.V. Khotkevich, S.V. Morozov, A.K. Geim, Two-dimensional atomic crystals, *Proceedings of the National Academy of Sciences of the United States of America* 102 (2005) 10451–10453.
 30. Y.H. Wu, T. Yu, Z.X. Shen, Two-dimensional carbon nanostructures: fundamental properties, synthesis, characterization, and potential applications, *Journal of Applied Physics* 108 (2010) 071301–0713039.
 31. L.M. Viculis, J.J. Mack, R.B. Kaner, A chemical route to carbon nanoscrolls, *Science* 299 (2003) 1361–1365.
 32. W.D. Heer, C. Berger, X. Wu, P.N. First, E.H. Conrad, X. Li, T. Li, M. Sprinkle, J. Hass, M.L. Sadowski, M. Potemski, G. Martinez, Epitaxial graphene, *Solid State Communications* 143 (2007) 92–100.
 33. Y.M. Chang, H. Kim, J.H. Lee, Y.W. Song, Multi layered graphene efficiently formed by mechanical exfoliation for nonlinear saturable absorbers in fiber mode-locked lasers, *Applied Physics Letters* 97 (2010) 211102–211105.
 34. A. Shukla, R. Kumar, J. Mazher, A. Balan, Graphene made easy: high quality large-area samples, *Solid State Communications* 149 (2009) 718–721.
 35. C. Nethravathi, M. Rajamathi, Chemically modified graphene sheets produced by the solvothermal reduction of colloidal dispersions of graphite oxide, *Carbon* 46 (2008) 1994–1998.
 36. C.L. Wong, M. Annamalai, Z.Q. Wang, M. Palaniapan, Characterization of nanomechanical graphene drum structures, *Journal of Micromechanics and Microengineering* 20 (2010) 115029–115034.
 37. Z. Tang, J. Zhuang, X. Wang, Exfoliation of graphene from graphite and their self-assembly at the oil-water interface, *Langmuir* 26 (2010) 9045–9049.
 38. S. Park, J. An, A.J.R. Potts, A. Velamakanni, S. Murali, R.S. Ruoff, Hydrazine-
-

- reduction of graphite- and graphene oxide, *Carbon* 49 (2011) 3019–3023.
39. H. Hiura, T.W. Ebbesen, J. Fujita, K. Tanigaki, T. Takada, Role of sp³ defect structures in graphite and carbon nanotubes, *Nature* 367 (1994) 148–151.
 40. J. Hass, W.A. Heer, E.H. Conrad, The growth and morphology of epitaxial multilayer graphene, *Journal of Physics: Condensed Matter* 20 (2008) 323202–323213.
 41. D. Gunlycke, P.E. Sheehan, Local peeling of graphene, *Science* 331 (2011) 1146–1147.
 42. O.O. Kit, T. Tallinen, L. Mahadevan, J. Timonen, P. Koskinen, Twisting graphene nanoribbons into carbon nanotubes, *Physics Review B* 85 (2012) 85428–85436.
 43. M. Lotya, Y. Hernandez, P.J. King, R.J. Smith, V. Nicolosi, L.S. Karlsson, F.M. Blighe, S. De, Z. Wang, I.T. McGovern, G.S. Duesberg, J.N. Coleman, Liquid phase production of graphene by exfoliation of graphite in surfactant/water solutions, *Journal of American Chemical Society* 131 (2009) 3611–3620.
 44. L.M. Viculis, J.J. Mack, O.M. Mayer, H.T. Hahn, R.B. Kaner, Intercalation and exfoliation routes to graphite nanoplatelets, *Journal of Materials Chemistry* 15 (2005) 974–978.
 45. X. Li, W. Cai, L. Colombo, R.S. Ruoff, Evolution of graphene growth on Ni and Cu by carbon isotope labeling, *Nano Letters* 9 (2009) 4268–4272.
 46. M.G. Rybin, A.S. Pozharov, E.D. Obraztsova, Control of number of graphene layers grown by chemical vapor deposition, *Physica Status Solidi C* 7 (2010) 2785–2788.
 47. A.L.V. Parga, F. Calleja, B. Borca, M.C.G. Passeggi Jr., J.J. Hinarejos, F. Guinea, R. Miranda, Periodically rippled graphene: growth and spatially resolved electronic structure, *Physics Review Letters* 100 (2008) 056807–0568011.
 48. M. Zheng, K. Takei, B. Hsia, H. Fang, X. Zhang, N. Ferralis, H. Ko, Y.L. Chueh, Y. Zhang, R. Maboudian, A. Javey, Metal-catalyzed crystallization of amorphous carbon to graphene, *Applied Physics Letters* 96 (2010) 063110–063115.
 49. S. Stankovich, D.A. Dikin, R.D. Piner, K.A. Kohlhaas, A. Kleinhammes, Y. Jia, Y. Wu, S.T. Nguyen, R.S. Ruoff, Synthesis of graphene-based nanosheets via chemical reduction of exfoliated graphite oxide, *Carbon* 45 (2007) 1558–1565.
 50. L. Gomez, Y. Zhang, A. Kumar, C. Zhou, Synthesis, transfer, and devices of single- and few-layer graphene by chemical vapor deposition, *IEEE Transactions on Nanotechnology* 8 (2009) 135–139.
 51. C. Soldano, A. Mahmood, E. Dujardin, Production, properties and potential of graphene, *Carbon* 48 (2010) 2127–2150.
 52. J.W. Suk, A. Kitt, C. Magnuson, Y. Hao, S. Ahmed, J. An, A.K. Swan, B.B. Gold-

- berg, R.S. Ruoff, Transfer of CVD-grown monolayer graphene onto arbitrary substrates, *ACS Nano* 5 (2011) 6916–6924.
53. D.R. Dreyer, S. Park, C.W. Bielawski, R.S. Ruoff, The chemistry of graphene oxide, *Chemical Society Reviews* 39 (2010) 228–240.
54. L. Zhang, J. Liang, Y. Huang, Y. Ma, Y. Wang, Y. Chen, Size-controlled synthesis of graphene oxide sheets on a large scale using chemical exfoliation, *Carbon* 47 (2009) 3365–3368.
55. J. Shen, Y. Hu, M. Shi, X. Lu, C. Qin, C. Li, M. Ye, Fast and facile preparation of graphene oxide and reduced graphene oxide nanoplatelets, *Chemistry of Materials* 21 (2009) 3514–3520
56. C. Daniela, V.D. Marcano, J.M. Kosynkin, J.M. Berlin, A. Sinitskii, Z. Sun, A. Slesarev, L.B. Alemany, W. Lu, M.J.M. Tour, Improved synthesis of graphene oxide, *ACS Nano* 4 (2010) 4806–4814.
57. S. Park, Y. Hu, J.O. Hwang, E.S. Lee, L.B. Casabianca, W. Cai, J.R. Potts, H.W. Ha, S. Chen, J. Oh, Junghoon, S.O. Kim, Y.H. Kim, Y. Ishii, R.S. Ruoff, Chemical structures of hydrazine-treated graphene oxide and generation of aromatic nitrogen doping, *Nature Communication* 3 (2012), 638–636.
58. H.J. Park, J. Meyer, S. Roth, Viera Skakalova, Growth and properties of few- layer graphene prepared by chemical vapor deposition, *Carbon* 46 (2010) 1088–1094.